Dual-Directional Magnetic Field Coupling Regulation on Vortex Division and Energy Storage Performance in Nanoparticle-Metal foam Composite Phase Change Material

Zhuotao Li, Yijie Zhuang* and Meiying He

School of Environmental Science and Engineering, Guangdong University of Technology, Guangzhou, 510006, China

Abstract: In this study, numerical simulations are conducted to investigate the regulation mechanism of the melting process and the regulation laws of energy storage performance of nano-enhanced phase change materials (NEPCMs) composite with metal foam under the coupling of magnetic convection induced by dual-directional magnetic fields and natural convection. The heat capacity-porosity method, Darcy-Forchheimer model and local thermal non-equilibrium model are adopted to describe the melting process, flow in porous media and coupled heat transfer, respectively. The effects of z-direction magnetic numbers (Mn) $(0 \leq \mathrm{Mn} \leq 6\times10^6)$ and y-direction magnetic numbers $(0 \leq \mathrm{Mn} \leq 6\times10^6)$ on the formation and differentiation of vortices, melting heat transfer and energy storage characteristics of non-Newtonian fluids are discussed. It is found that the application of a magnetic field can effectively promote the melting of NEPCM melts. However, the competition between the dual-directional magnetic fields will mutually inhibit their promoting effects. This inhibitory effect further affects the heat transfer performance by disrupting the vortex structure and the morphology of the y-direction Kelvin force. Although the addition of y and z-direction magnetic fields leads to competition, different combinations of magnetic field intensity parameters result in distinct heat storage characteristics that do not simply increase or decrease monotonically.

Keywords: Vortex division, dual-direction magnetic field, Kelvin force, Metal foam, Nano-enhanced phase change material.

1. INTRODUCTION

Latent heat thermal energy storage (LHTES) technology based on phase change materials (PCMs) is a research direction of great significance, with wide applications in precision electronic devices, battery thermal management, waste heat recovery systems, and the aerospace field. There are several mainstream approaches to solve the problems of poor thermal conductivity of PCMs and the difficulty in regulating the phase change heat transfer process.

Some researchers choose to couple porous media with PCMs. Metal foams made of high thermal conductivity materials can be effectively coupled with PCMs, enabling more uniform enhancement of the composite phase change heat transfer system [1]. Nanoparticles are also effective materials for improving the internal heat transfer properties of PCMs [2]. Heidari *et al*. [3] investigated the forced convective heat transfer of hybrid nanofluids in channels using numerical methods, and the study mentioned that the weakening of convective effects was related to the influence of viscosity. During the phase change process, interactions between nanoparticles and those between nanoparticles and liquids may induce complex non-Newtonian rheological behaviors. Therefore, the design of nano-enhanced phase change materials (NEPCMs) should consider the influence of non-Newtonian effects [4, 5].

In addition, introducing external magnetic fields to regulate the phase change process has attracted the attention of many scholars in recent years. Ali *et al*. [6] carried out a numerical study on the magnetohydrodynamic (MHD) transient flow of nanofluids in a rotating frame, and found that an increase in the magnetic parameter reduces the flow velocity but increases the fluid temperature. In terms of the magnetic field regulation mechanism, the magnitude of the Rayleigh number (Ra) affects the regulation effect of the magnetic field. Xu *et al*. [7] demonstrated that the Kelvin force distribution presents force loop or force bridge configurations under varying Ra numbers. The force loop can make the melting interface more parallel to the heating side, while the force bridge weakens the natural convection in the upper region and inhibits heat transfer. Zhuang *et al*. [8] studied the magnetic field regulation mechanism during the melting process of non-Newtonian ferromagnetic nano-enhanced phase change systems at low Ra numbers.

One motivation for the current research is that the analysis of the coupled interaction and regulation mechanism between complex magnetic convection driven by multi-directional magnetic fields and natural

*Address correspondence to this author at School of Environmental Science and Engineering, Guangdong University of Technology, Guangzhou, 510006, China; E-mail: zyj7933@gdut.edu.cn

convection is insufficient, and it is necessary to further study the mechanism by which the Kelvin force affects the phase change process. Current studies have shown that the strategy of applying an external magnetic field is a feasible method for regulating the phase change process of NEPCMs, but the magnetic field regulation mechanism for complex magnetic field coupling with natural convection has not been extensively studied.

The innovation of this study lies in considering both dual-directional magnetic fields and the gravitational field simultaneously, and using a three-dimensional numerical model to describe the effect of dual-directional magnetic fields on the melting process of a non-Newtonian phase change thermal energy storage system under normal gravity. In our previous studies [8], it was found that the unidirectional magnetic field mostly exhibits a monotonic inhibitory or promotional effect related to the magnetic number (Mn) in regulating the melting outcome. The competitive effect of multi-directional magnetic fields can effectively eliminate the monotonic relationship between the melting performance and the magnetic number, and different magnetic strengths can also induce phase change materials (PCMs) to exhibit distinct melting characteristics. Research on the regulatory mechanism of complex magnetic fields is conducive to designing more appropriate magnetic fields for practical applications. In this study, two mutually orthogonal uniform magnetic fields are added to a square cavity, one parallel to the heating side and the other in the same direction as the melting interface advancement. By comparing the effects of different Mn combinations of the dual-directional magnetic fields on phase change, the competitive relationship and mechanism of the dual-directional Kelvin force in influencing convection are investigated. In addition, to avoid natural convection being too strong and dominating the liquid phase flow, this study is set under low Ra conditions, aiming to explore the phase change heat transfer regulation mechanism of the coupling between dual-directional Kelvin forces and buoyancy. Our theoretical findings may provide a theoretical basis for further specific engineering designs, such as thermal management of unmanned aerial vehicles, building energy efficiency, and thermal control of spacecraft.

2. MATHEMATICAL MODEL

2.1. Problem Statement

Figure **1** shows the physical model of a LHTES unit. Two composite uniform magnetic fields, one along the y-axis and the other along the z-axis, are located outside the rectangular cavity. The magnetic field in the y-direction is perpendicular to the heating surface and aligned with the direction of the heat source. The magnetic field in the z-direction is parallel to the direction of gravity but opposite to it. The cavity is filled with NEPCM coupled with copper foam; the left wall serves as a constant-temperature heat source, and the remaining surfaces are adiabatic. The relevant thermophysical parameters of paraffin, copper foam, and Fe_3O_4 nanoparticles used in this study are presented in Table **1**. The thermophysical properties of copper foam and Fe_3O_4 nanoparticles are adopted from those of copper and Fe_3O_4, respectively [9, 10].

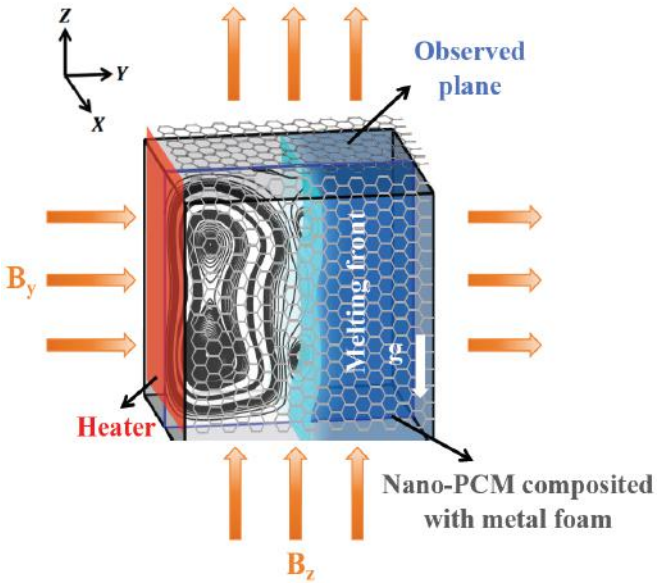

Figure 1: Schematic diagram of the LHTES unit.

In this study, liquid paraffin is assumed to be an incompressible fluid, and changes in its heat capacity, thermal conductivity, and latent heat during the melting process are neglected. Paraffin is treated as an insulator, so no conduction current is generated in the fluid. The relationship between magnetization and temperature is considered linear. Copper foam and paraffin are regarded as continuous media, and the interaction between the magnetic field and the metal foam is ignored. The local thermal non-equilibrium (LTNE) model is employed to describe the transient thermal energy interaction between paraffin and copper foam.

2.2. Governing Equations

Natural convection driven by mass transfer within the three-dimensional computational domain is governed by the continuity, momentum, and mass

Table 1: Thermophysical Properties of Paraffin, Copper and Fe_3O_4 [7, 11].

Properties	Paraffin	Copper	Fe_3O_4
Density (kg/m^3)	780 (liquid)	8920	5200
Dynamic viscosity (kg/m s)	0.000385	-	-
Specific heat capacity (J/kg K)	2196	380	670
Latent heat (kJ/kg)	119.40	-	-
Thermal expansion coefficient	0.00091	-	-
Thermal conductivity (Wm/K)	0.23 (solid) 0.1 (liquid)	401	80
Melting temperature (K)	300.81-307.5	-	-

transfer equations, whose dimensionless forms are expressed as follows:

$$\nabla \cdot \dot{U} = 0, \tag{1}$$

$$\frac{1}{\varphi}\frac{\partial U}{\partial F_o} + \frac{1}{\varphi^2}\left(\frac{U\partial U}{\partial X} + \frac{V\partial U}{\partial Y} + \frac{W\partial U}{\partial Z}\right) = -\frac{1}{E}\frac{\partial P}{\partial X} + \frac{FPr^*}{\varphi E}\left(\frac{\partial \tau_{XX}}{\partial X} + \frac{\partial \tau_{XY}}{\partial Y} + \frac{\partial \tau_{XZ}}{\partial Z}\right) - \left(\frac{F\overline{\mu}Pr^*}{EDa} + \frac{C}{\sqrt{Da}}\sqrt{U^2+V^2+W^2}\right)U - S_\theta U, \tag{2}$$

$$\frac{1}{\varphi}\frac{\partial V}{\partial F_o} + \frac{1}{\varphi^2}\left(\frac{U\partial V}{\partial X} + \frac{V\partial V}{\partial Y} + \frac{W\partial V}{\partial Z}\right) = -\frac{1}{E}\frac{\partial P}{\partial Y} + \frac{FPr^*}{\varphi E}\left(\frac{\partial \tau_{XY}}{\partial X} + \frac{\partial \tau_{YY}}{\partial Y} + \frac{\partial \tau_{ZY}}{\partial Z}\right) - \left(\frac{F\overline{\mu}Pr^*}{EDa} + \frac{C}{\sqrt{Da}}\sqrt{U^2+V^2+W^2}\right)V - S_\theta V - \overline{M}\cdot Mn\frac{\partial \theta_{nf}}{\partial Y}, \tag{3}$$

$$\frac{1}{\varphi}\frac{\partial W}{\partial F_o} + \frac{1}{\varphi^2}\left(\frac{U\partial W}{\partial X} + \frac{V\partial W}{\partial Y} + \frac{W\partial W}{\partial Z}\right) = -\frac{1}{E}\frac{\partial P}{\partial Z} + \frac{FPr^*}{\varphi E}\left(\frac{\partial \tau_{XZ}}{\partial X} + \frac{\partial \tau_{YZ}}{\partial Y} + \frac{\partial \tau_{ZZ}}{\partial Z}\right) - \left(\frac{F\overline{\mu}Pr^*}{EDa} + \frac{C}{\sqrt{Da}}\sqrt{U^2+V^2+W^2}\right)W - S_\theta W - \overline{M}\cdot Mn\frac{\partial \theta_{nf}}{\partial Z} + Ra\cdot Pr\cdot\theta_{nf}, \tag{4}$$

$$\left[\varepsilon + \frac{\varepsilon}{Ste}\frac{d(f)}{d(\theta_{nf})}\right]\frac{\partial \theta_{nf}}{\partial Fo} + \left(U\frac{\partial \theta_{nf}}{\partial X} + V\frac{\partial \theta_{nf}}{\partial Y} + W\frac{\partial \theta_{nf}}{\partial Z}\right) = \left(\frac{\partial^2\theta_{nf}}{\partial X^2} + \frac{\partial^2\theta_{nf}}{\partial Y^2} + \frac{\partial^2\theta_{nf}}{\partial Z^2}\right) + Sp\left(\theta_s - \theta_{nf}\right), \tag{5}$$

$$(1-\varepsilon)\frac{\partial \theta_s}{\partial Fo} = \frac{1}{\xi}\left(\frac{\partial^2\theta_s}{\partial X^2} + \frac{\partial^2\theta_s}{\partial Y^2} + \frac{\partial^2\theta_s}{\partial Z^2}\right) + \xi_\rho\xi_{cp}Sp\left(\theta_s - \theta_{nf}\right), \tag{6}$$

Mn, Da, Ste, Pr, Ra and Re represent the Magnetic number, Darcy number, Stefan number, Prandtl number Rayleigh number and Reynolds number, respectively. Mn reflects the dimensionless magnetic field strength. Da characterizes the permeability of porous media. Ste represents the ratio of sensible heat to latent heat. Pr denotes the ratio of momentum diffusion capacity to heat diffusion capacity. Ra indicates the relative magnitude of buoyancy force to viscous force. Re reflects the ratio of inertial force to viscous force. Detailed theoretical explanations of the governing equations can be found in our previous studies [8].

The initial conditions are as follows:

$$Fo = 0, U = V = W = 0, \theta_{nf} = \theta_s = \theta_\infty = 0, \theta_h = 1. \tag{7}$$

The boundary conditions of the cubical cavity are as follows:

$$Fo > 0,\ Y = 0,\ 0 \le X \le N,\ 0 \le Z \le N,\ \theta_{nf} = \theta_s = \theta_h = 1, \tag{8}$$

$$Fo > 0,\ Y = N,\ 0 \le X \le N,\ 0 \le Z \le N,\ \frac{\partial \theta_{nf}}{\partial X} = \frac{\partial \theta_{nf}}{\partial Z} = \frac{\partial \theta_S}{\partial X} = \frac{\partial \theta_S}{\partial Z} = 0, \tag{9}$$

$$Fo > 0,\quad X = 0\ or\ N,\quad 0 \le Y \le N,\quad 0 \le Z \le N,\quad \frac{\partial \theta_{nf}}{\partial Y} = \frac{\partial \theta_{nf}}{\partial Z} = \frac{\partial \theta_S}{\partial Y} = \frac{\partial \theta_S}{\partial Z} = 0, \tag{10}$$

$$Fo > 0,\quad Z = 0\ or\ N,\quad 0 \le X \le N,\quad 0 \le Y \le N,\quad \frac{\partial \theta_{nf}}{\partial X} = \frac{\partial \theta_{nf}}{\partial Y} = \frac{\partial \theta_S}{\partial X} = \frac{\partial \theta_S}{\partial Y} = 0. \tag{11}$$

To evaluate the heat storage performance of NEPCM, the definitions of the indicators for assessing heat storage capacity are as follows:

$$Nu = -\frac{\partial \theta_{nf}}{\partial Y}|_{Y=0}, \tag{12}$$

$$\overline{Nu} = \int_{Z=0}^{L}\int_{X=0}^{L}|Nu|dXdZ, \tag{13}$$

$$E(t) = E_{nf}(t) + E_s(t), \tag{14}$$

$$E_{nf}(t) = \begin{cases} m_{nf}c_{nf}(T_{ave}(t) - T_\infty), T \le T_{m1} \\ m_{nf}c_{nf}\left(T_{nf_{ave}}(t) - T_\infty\right) + m_{nf}L_{nf}, T > T_{m1} \end{cases}, \tag{15}$$

$$E_s(t) = m_s c_s\left(T_{s_{ave}}(t) - T_\infty\right), \tag{16}$$

$$E_S(t) = m_{nf}c_{nf}\left(T_{nf_{ave}}(t) - T_\infty\right) + m_s c_s\left(T_{s_{ave}}(t) - T_\infty\right), \tag{17}$$

$$E^* = \frac{E}{E_{ref}}, E_s^* = \frac{E_S}{E_{S_{ref}}}, \tag{18}$$

$$Q = \frac{E(t_{total})}{t_{total}}, Q^* = \frac{Q}{Q_{ref}}, \tag{19}$$

where E^*, E_s^* and Q^* represent the non-dimensional total heat storage, non-dimensional sensible heat

storage and non-dimensional heat storage efficiency, respectively. The subscript 'ref' denotes the reference case.

3. NUMERICAL METHOD AND VALIDATION

3.1. Numerical Method

The numerical simulation employs an iterative finite volume method with a three-dimensional staggered grid, coupled to the SIMPLE algorithm. Velocity components are at cell face midpoints, scalars pressure, temperature at cell centers. Transient terms use forward difference, convective terms second-order upwind, and diffusive terms central difference.

3.2. Validation

Figure **2a** presents the grid number and time step independence analyses. For the computational domain, three grid configurations (39,304, 46,656 and 54,872 cells) and three time steps (1×10^{-6} s, 1×10^{-5} s and 2×10^{-5} s) were tested separately. To balance computational efficiency and solution accuracy, a grid with 46,656 cells and a time step of 1×10^{-5} s are adopted in this study to simulate the phase change heat transfer process for all cases. Figure **2b** compares the evolution of the melting front in the magnetic field experimental system with the numerical simulation results. Throughout the entire melting process, the numerical results are in good agreement with the experimental results, which indicates that the employed numerical model and computational code are reliable.

4. RESULTS AND DISCUSSION

Figures **3a** and **3b** show the streamline diagrams and velocity field diagrams for Mn_z and Mn_y ranging from 0 to 6×10^6, respectively. As can be seen from Figure **3a**, the y-direction magnetic field longitudinally splits the large vortex in the absence of a magnetic field, dividing it into multiple rows of small vortices. This phenomenon becomes more pronounced with the increase of Mn_y, and the arrangement of small vortices becomes more regular. In contrast, the z-direction magnetic field transversely cuts the original large vortex and forms several small vortices around the split large vortex accordingly.

Under the coupling of y and z-direction magnetic fields, the streamlines exhibit four morphologies. When the y and z-direction magnetic fields are both small and of similar magnitude, as shown in the gray zone, the z-direction magnetic field disrupts the multi-row small vortex morphology formed by the y-direction magnetic field. At this time, the coupling of the two magnetic fields causes the streamlines to form a single-vortex morphology similar to that in the absence of a magnetic field. When the y-direction magnetic field is stronger

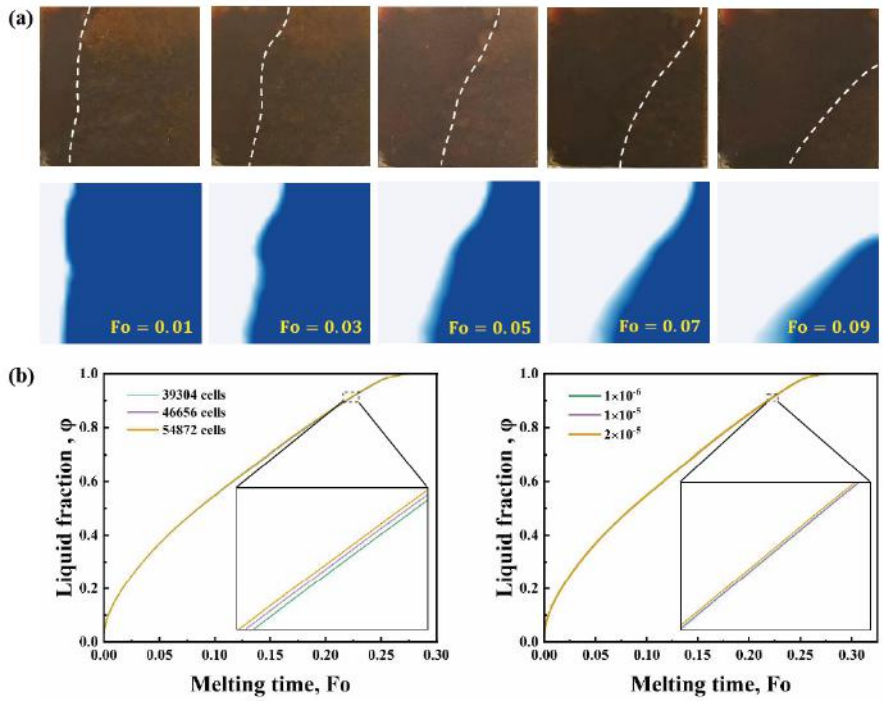

Figure 2: (**a**) Independent analyses under different grid numbers and time steps; (**b**) comparison of melting interface profiles between numerical and experimental results under a uniform magnetic field.

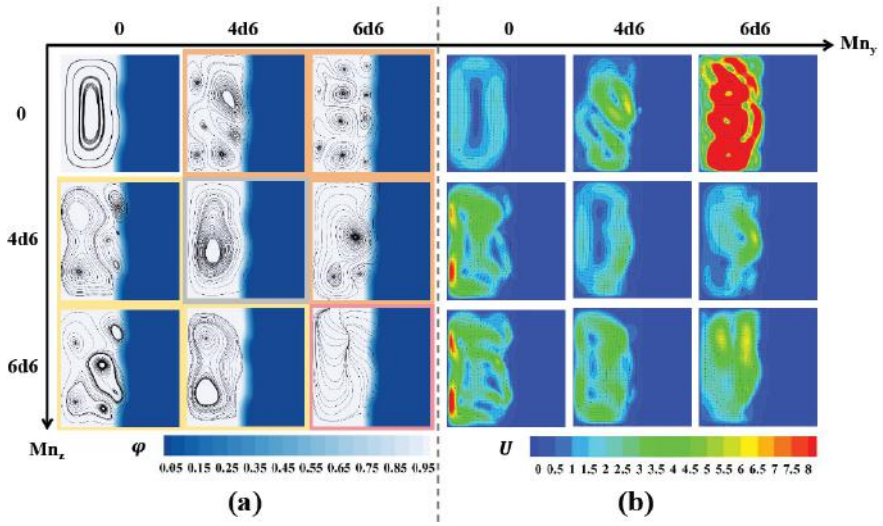

Figure 3: Comparison of (**a**) streamlines and (**b**) velocity field for Mn_z from 0 to 6×10^6 and Mn_y from 0 to 6×10^6 at Fo = 0.08 and $Ra = 10^3$.

than the z-direction magnetic field, as shown in the orange zone, the morphology of streamlines in the flow field is dominated by the y-direction magnetic field, presenting a multi-vortex structure with longitudinal differentiation, although the presence of the large vortex is still quite obvious at this time. When the z-direction magnetic field is stronger than the y-direction one, as shown in the yellow zone, the morphology of streamlines in the flow field is mainly affected by the z-direction magnetic field, showing the unique differentiation mode of the z-direction magnetic field in the large vortex. When both the y and z-direction magnetic fields are strong, as shown in the red zone, the magnetic convection induced by the y and z-direction magnetic fields collides violently and rolls upward, forming vertical vortices.

It can be found in Figure **3b** that the velocity distribution in the liquid phase is closely related to the morphology of vortices. A comparison of the streamline diagrams and velocity field diagrams reveals that the flow velocity of the single vortex is the slowest, and the role of thermal convection in heat transfer is relatively small at this time. With the increase in the number of differentiated small vortices, the average velocity in the liquid phase becomes higher and higher. This is because the convection induced by the edges of multiple vortices can significantly increase the velocity in the flow field. The enhanced fluid mobility also strengthens heat transfer, and this promoting effect on heat transfer can ultimately lead to a significant improvement in heat storage efficiency. In the vertical vortices in the red zone, the average velocity of the velocity field is not as high as that in the case where only the y-direction magnetic field is 6×10^6. This indicates that although the magnetic convection is more intense at this time and collides with each other to generate vertical vortices that deviate from the plane of the two magnetic field directions, the promotion of thermal convection by these vertical vortices is not as effective as the uniform and stable multi-vortex structure generated by the single y-direction magnetic field.

Figures **4a** and **4b** show the z-direction Kelvin force field and y-direction Kelvin force field under different combinations of Mn_y and Mn_z parameters, respectively. In the z-direction Kelvin force field of Figure **4a**, it can be seen that the increase of the z-direction magnetic field mainly affects the magnitude of the Kelvin force in the z-direction. Only in two cases, $Mn_y = 5\times10^6$ and $Mn_y = 6\times10^6$, the addition of the z-direction magnetic field disconnects the two originally connected negative Kelvin force regions and makes the division of positive and negative Kelvin force regions clearer. The increase of the y-direction magnetic field, however, affects the angle of the positive and negative regions in the z-direction Kelvin force field. From left to right, as the y-direction magnetic field increases, the included angle between the four regions in the z-direction Kelvin force and the bottom edge becomes larger and larger. In Figure **4b**, it can be seen that in the absence of the z-direction magnetic field, the force loops of the y-direction Kelvin force are gradually formed with the increase of the y-direction magnetic field. The addition of the z-direction magnetic field disrupts the formation of force loops, just as it disrupts the formation of small vortices in the velocity field. Under the influence of the

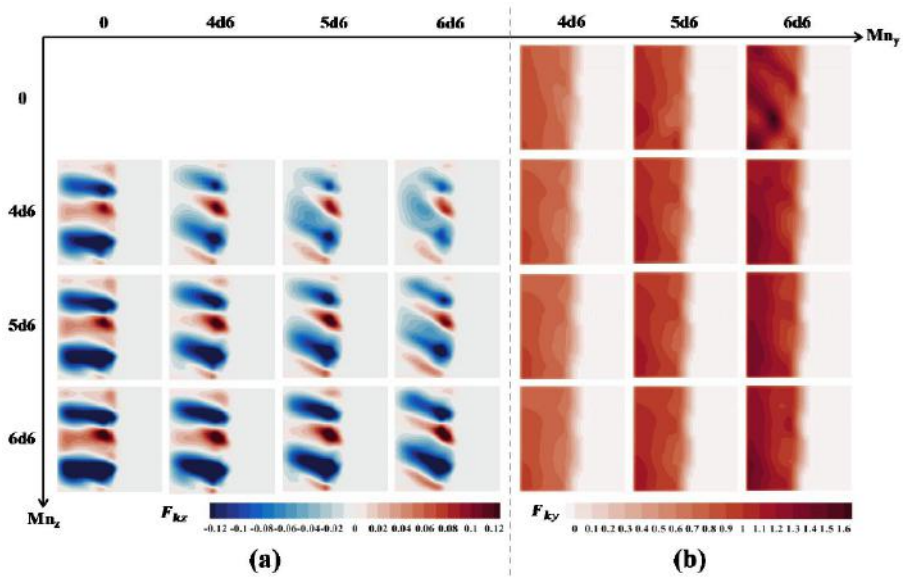

Figure 4: Comparisons of (**a**) z-direction Kelvin force field and (**b**) y-direction Kelvin force field for Mn_y from 0 to 6×10^6 and Mn_z from 0 to 6×10^6 at Fo = 0.08 and $\mathrm{Ra} = 10^3$.

z-direction magnetic field, the y-direction Kelvin force gradually converges into a high Kelvin force region on the left, forming a force column morphology.

Figures **5a** and **5b** show the variation of liquid fraction with time and the variation of average Nusselt number $(\overline{Nu})$ with time under different Mn_y and Mn_z parameters, respectively. From the liquid fraction - time curve, it can be seen that compared with the baseline case without any magnetic field, the application of a magnetic field effectively accelerates melting and shortens the melting time. Among them, the addition of the magnetic field with $\mathrm{Mn_y} = 6\times10^6$ can significantly shorten the melting time. However, the addition of the z-direction magnetic field at this time will inhibit the promoting effect of the y-direction magnetic field. This is related to the competition between the z-direction and y-direction magnetic fields mentioned earlier, which

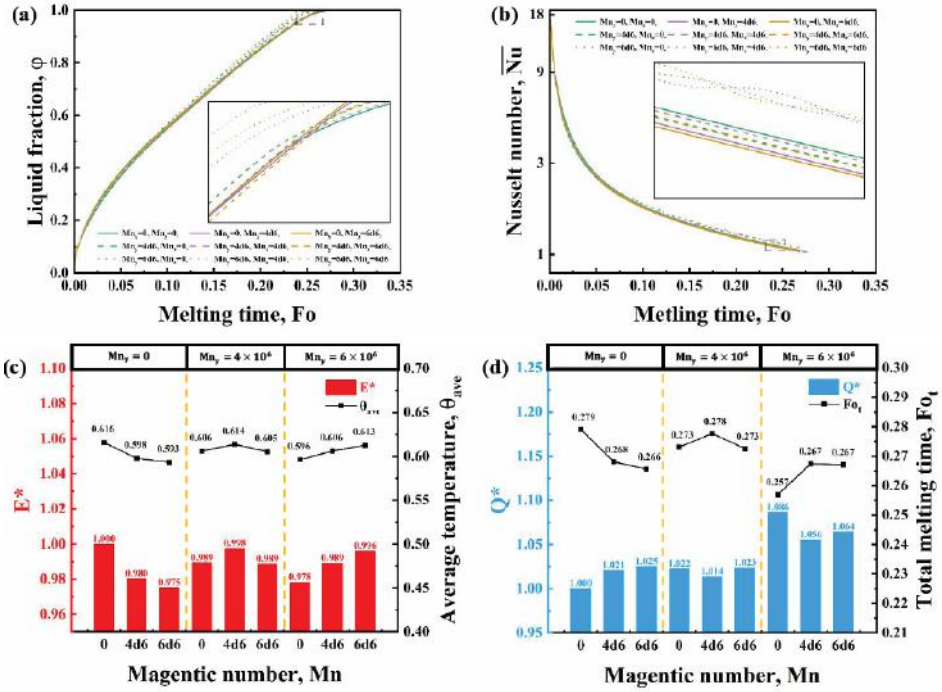

Figure 5: (**a**) Variations of liquid fraction with Fo for different Mn_y and Mn_z; (**b**) Variations of average Nusselt number with Fo for different Mn_y and Mn_z; (**c**) Variations of average temperature and total heat storage for different Mn_y and Mn_z; (**d**) Variations of total melting time and heat storage efficiency for different Mn_y and Mn_z.

disrupts the multi-vortex structure formed by the y-direction magnetic field. In the case where $\mathrm{Mn_y} = 4\times10^6$ is coupled with the z-direction magnetic field, the promoting effect of the magnetic field is not as obvious as that of the single z-direction magnetic field. This is because when $\mathrm{Mn_y} = 4\times10^6$, the competition between the z-direction and y-direction magnetic fields reduces the original multi-vortex structure of the y-direction magnetic field to a single-vortex structure similar to that without a magnetic field. Although the z-direction magnetic field dominates the streamline morphology when $\mathrm{Mn_z} = 6\times10^6$, the number of vortices is still smaller than that in the two cases with only the z-direction magnetic field. Therefore, the promoting effect of the magnetic field on melting at this time is not as significant as that of the single z-direction magnetic field. From Figure **5b**, it can be seen that only the three cases with the magnetic field of $\mathrm{Mn_y} = 6\times10^6$ show oscillations in the $\overline{Nu}$ in the later stage of melting. Such oscillations may be due to the stronger magnetic force causing more prominent disturbance of the nanofluid on the heating wall, thereby disrupting the stable convective heat transfer.

Figure **5c** shows the heat storage and average temperature under different $\mathrm{Mn_y}$ and $\mathrm{Mn_z}$ parameters. In the absence of the y-direction magnetic field, an increase in the z-direction magnetic field reduces the total heat storage of the system. However, under different y-direction magnetic fields, an increase in the z-direction magnetic field leads to different effects. When $\mathrm{Mn_y} = 4\times10^6$, an increase in the z-direction magnetic field first increases and then decreases the heat storage. When $\mathrm{Mn_y} = 6\times10^6$, an increase in the z-direction magnetic field causes a monotonic increase in heat storage. The different effects exhibited by these multiple parameter combinations are related to the magnetic field competition mentioned earlier. The competition of magnetic fields with different parameters leads to the differentiation of different vortex morphologies, and different thermal convection states during the melting process result in different heat storage capacities.

Figure **5d** shows the heat storage efficiency and total melting time under different $\mathrm{Mn_y}$ and $\mathrm{Mn_z}$ parameters. It can be seen that in the cases with only the z-direction magnetic field, an increase in the z-direction magnetic field leads to a monotonic increase in heat storage efficiency and a monotonic decrease in total melting time. When $\mathrm{Mn_y} = 4\times10^6$, an increase in the z-direction magnetic field first increases the total melting time and then decreases it to the level of the case without the z-direction magnetic field. Although the heat storage increases when $\mathrm{Mn_y} = 4\times10^6$ and $\mathrm{Mn_z} = 4\times10^6$, the overall heat storage efficiency is still lower than that of the case without the z-direction magnetic field due to the longer total melting time. When $\mathrm{Mn_y} = 6\times10^6$, although the total melting time is the same for $\mathrm{Mn_z} = 4\times10^6$ and $\mathrm{Mn_z} = 6\times10^6$, an increase in Mnz can improve the heat storage capacity of the system, so the heat storage efficiency of the case with $\mathrm{Mn_y} = 6\times10^6$ and $\mathrm{Mn_z} = 6\times10^6$ is improved.

Comparing the total melting time and heat storage efficiency of all nine cases, although the competition between the dual-directional magnetic fields leads to mutual inhibition of their original promoting effects, the application of magnetic fields always accelerates the melting process compared with the case without a magnetic field, despite variations in the promoting effects among different magnetic field parameters.

5. CONCLUSION

1) The coupling of y-direction and z-direction magnetic fields with medium and low intensities leads to competition between the two magnetic fields, thereby disrupting the magnetic convection characteristics induced by each magnetic field. In contrast, high-intensity magnetic fields cause liquid NEPCM to form vertical vortices.

2) The total melting time is closely related to the number and morphology of vortices. The increased liquid phase velocity induced by the multi-vortex structure can effectively enhance convective heat transfer and thus promote the melting process.

3) In terms of magnetic field morphology, the force loops of the y-direction Kelvin force are also disrupted by the z-direction magnetic field. As the z-direction magnetic field increases, the force loops gradually disappear and transform into force columns.

4) The coupling of y-direction and z-direction magnetic fields exerts complex effects on the melting of NEPCM. For heat storage and heat storage efficiency, their increase or decrease depends on the competition between the dual-directional magnetic fields. Different dual-directional magnetic field parameters result in distinct heat storage characteristics.

In general, if a component in an aerospace thermal system requires high heat dissipation efficiency, the introduction of a magnetic field may significantly enhance the heat storage efficiency of NEPCM. However, at the same time, we do not want NEPCM to sacrifice excessive heat storage capacity. In such cases, the addition of a dual-direction magnetic field can effectively maintain a certain level of heat storage efficiency without reducing the heat storage capacity too much.

REFERENCES

[1] Zhang S, Feng D, Shi L, Wang L, Jin Y, Tian L, Li Z, Wang G, Zhao L, Yan Y. A review of phase change heat transfer in shape-stabilized phase change materials (ss-PCMs) based on porous supports for thermal energy storage. Renewable and Sustainable Energy Reviews 2021; 135: 110127. https://doi.org/10.1016/j.rser.2020.110127

[2] Zhuang Y, Lin J, Liu A. Numerical investigation on non-Newtonian melting heat transfer of phase change material composited with nanoparticles and metal foam in an inner heated cubic cavity. Journal of Energy Storage 2022; 51: 104417. https://doi.org/10.1016/j.est.2022.104417

[3] Heidari H, Mohebbi R, Kazemi A. Forced convection heat transfer of Ag–MgO/water micropolar hybrid nanofluid inside a stairway channel. International Journal of Modern Physics C 2021; 32(11): 2150147. https://doi.org/10.1142/S0129183121501473

[4] Liu Z, Huang S-M, Wang C, Zhuang Y. A review on non-Newtonian effects and structure-activity relationship of nanoparticles enhanced phase change materials in porous media. Journal of Energy Storage 2023; 64: 107221. https://doi.org/10.1016/j.est.2023.107221

[5] Cui W, Li X, Li X, Lu L, Ma T, Wang Q. Combined effects of nanoparticles and ultrasonic field on thermal energy storage performance of phase change materials with metal foam. Applied Energy 2022; 309: 118465. https://doi.org/10.1016/j.apenergy.2021.118465

[6] Ali B, Hussain S, Nie Y, Hussein AK, Habib D. Finite element investigation of Dufour and Soret impacts on MHD rotating flow of Oldroyd-B nanofluid over a stretching sheet with double diffusion Cattaneo Christov heat flux model. Powder Technology 2021; 377: 439-452. https://doi.org/10.1016/j.powtec.2020.09.008

[7] Xu W, Huang T, Huang S-M, Zhuang Y. Regulation mechanism of magnetic field on non-Newtonian melting and energy storage performance of metal foam composite nano-enhanced phase change materials. International Journal of Heat and Mass Transfer 2023; 200: 123501. https://doi.org/10.1016/j.ijheatmasstransfer.2022.123501

[8] Zhuang Y, Huang T, Feng J-C. Oscillatory instability of magneto-convection during the melting of non-Newtonian ferromagnetic nano-enhanced phase change materials at low Rayleigh number. Applied Thermal Engineering 2024; 248: 123306. https://doi.org/10.1016/j.applthermaleng.2024.123306

[9] Nield DA, Bejan A. Convection in Porous Media, Springer, New York 2006.

[10] Tizakast Y, Kaddiri M, Lamsaadi M. Double-diffusive mixed convection in rectangular cavities filled with non-Newtonian fluids. International Journal of Mechanical Sciences 2021; 208: 106667. https://doi.org/10.1016/j.ijmecsci.2021.106667

[11] Xu W, Liu Z, Huang S-M, Zhuang Y. Evaluation and development of a predictive model for conjugate phase change heat transfer of energy storage system partially filled with porous media. Energy Storage and Saving 2022; 1(4): 293-308. https://doi.org/10.1016/j.enss.2022.08.001

Received on 03-11-2025 Accepted on 01-12-2025 Published on 19-12-2025